



**QUEEN'S  
UNIVERSITY  
BELFAST**

## Effects of Poly ( $\epsilon$ -caprolactone) Coating on the Properties of Three-Dimensional Printed Porous Structures

Zhou, Z., Lennon, A., Cunningham, E., Buchanan, F., Clarke, S., McCarthy, H., & Dunne, N. (2017). Effects of Poly ( $\epsilon$ -caprolactone) Coating on the Properties of Three-Dimensional Printed Porous Structures. *Journal of the Mechanical Behavior of Biomedical Materials*, 70(June 2017), 68-83.  
<https://doi.org/10.1016/j.jmbbm.2016.04.035>

### Published in:

Journal of the Mechanical Behavior of Biomedical Materials

### Document Version:

Peer reviewed version

### Queen's University Belfast - Research Portal:

[Link to publication record in Queen's University Belfast Research Portal](#)

### Publisher rights

© 2016 Elsevier Ltd. This manuscript version is made available under the CC-BY-NC-ND 4.0 license <http://creativecommons.org/licenses/by-nc-nd/4.0/>, which permits distribution and reproduction for non-commercial purposes, provided the author and source are cited.

### General rights

Copyright for the publications made accessible via the Queen's University Belfast Research Portal is retained by the author(s) and / or other copyright owners and it is a condition of accessing these publications that users recognise and abide by the legal requirements associated with these rights.

### Take down policy

The Research Portal is Queen's institutional repository that provides access to Queen's research output. Every effort has been made to ensure that content in the Research Portal does not infringe any person's rights, or applicable UK laws. If you discover content in the Research Portal that you believe breaches copyright or violates any law, please contact [openaccess@qub.ac.uk](mailto:openaccess@qub.ac.uk).

### Open Access

This research has been made openly available by Queen's academics and its Open Research team. We would love to hear how access to this research benefits you. – Share your feedback with us: <http://go.qub.ac.uk/oa-feedback>

# Effects of Poly ( $\epsilon$ -caprolactone) Coating on the Properties of Three-Dimensional Printed Porous Structures

Zuoxin Zhou <sup>1</sup>, Eoin Cunningham <sup>2</sup>, Alex Lennon<sup>2</sup>, Helen McCarthy <sup>3</sup>, Fraser Buchanan <sup>2</sup>, Nicholas Dunne <sup>2,4, \*</sup>

1. Warwick Manufacturing Group, University of Warwick, UK
2. School of Mechanical and Aerospace Engineering, Queen's University of Belfast, UK
3. School of Pharmacy, Queen's University Belfast, Lisburn Road, Belfast BT9 7BL, UK
4. School of Mechanical and Manufacturing Engineering, Dublin City University, Republic of Ireland

## ABSTRACT

Powder-based inkjet three-dimensional printing (3DP) to fabricate pre-designed 3D structures has drawn increasing attention. However there are intrinsic limitations associated with 3DP technology due to the weak bonding within the printed structure, which significantly compromises its mechanical integrity. In this study, calcium sulphate ceramic structures demonstrating a porous architecture were manufactured using 3DP technology and subsequently post-processed with a poly ( $\epsilon$ -caprolactone) (PCL) coating. PCL concentration, immersion time, and number of coating layers were the principal parameters investigated and improvement in compressive properties was the measure of success. Interparticle spacing within the 3DP structures were successfully filled with PCL material. Consequently the compressive properties, wettability, morphology, and *in vitro* resorption behaviour of 3DP components were significantly augmented. The average compressive strength, Young's modulus, and toughness increased 217%, 250%, and 315%, following PCL coating. Addition of a PCL surface coating provided long-term structural support to the host ceramic material, extending the resorption period from less than 7 days to a minimum of 56 days. This study has demonstrated that application of a PCL coating onto a ceramic 3DP structure was a highly effective approach to addressing some of the limitations of 3DP manufacturing and allows this advanced technology to be potentially used in a wider range of applications.

\*Corresponding Author: Tel.: +353 (0) 1 7005104

Email: [nicholas.dunne@dcu.ie](mailto:nicholas.dunne@dcu.ie) (N. Dunne).

Postal Address: School of Mechanical and Manufacturing Engineering, Dublin City University, Republic of Ireland.

## 1 Introduction

One of the challenges additive manufacturing (AM) technologies is facing today is to manufacture more robust components from a greater selection of materials. Powder-based inkjet three-dimensional printing (3DP) is one of the AM technologies that can potentially use a broad range of powdered materials to fabricate complex internal and external structures. It involves a sequential layering process, through which binder droplets are ejected from inkjet print head nozzles and selectively deposited on the powder bed to build a 3D component from a series of cross sections. Co-manufacturing a support structure to overhang printed features is not required. Thus, 3DP offers great flexibility in product design and material selection. Studies have investigated a wide variety of powdered materials processed in 3DP, including metal (Lim *et al.*, 2007; Williams *et al.*, 2007), ceramics (Peters *et al.*, 2006; Gbureck *et al.*, 2007; Zhou *et al.*, 2014), polymers (Lam *et al.*, 2002; Chia and Wu, 2015), wood (Saidin *et al.*, 2013), and their composites (Will *et al.*, 2008; Koltygin and Bazhenov, 2012; Zhou *et al.*, 2015). In practice, plaster calcium sulphate ( $\text{CaSO}_4$ ) powder is one of the most commonly used materials in 3DP manufacturing. This technology has been used for rapid prototyping, domestic use, architectural design, artwork and medical applications, such as tissue-engineering scaffolds (Iliescu *et al.*, 2009; D'aveni, 2013; Huson and Hoskins, 2014; Shirazi *et al.*, 2015).

There are still major limitations associated with 3DP technology due to inherent weak bonding within the printed structures, which yields poor mechanical performance (Chummanklang *et al.*, 2007). This inherent weak bonding is in part due to the large degree of interparticle spacing within the powder bed. During a 3DP process, the adjacent powders are only loosely connected by the deposited binder droplets. The weak bonding between the powder particles leads to interparticle spacing within the 3DP structure. Stress concentrations surrounding the interparticle spacing reduce the overall mechanical integrity of the printed structure. The initial green strength of a 3DP ceramic structure only comes from the mechanical interlocking of precipitated crystals (Butscher *et al.*, 2011). Poor mechanical properties have limited many potential applications for 3DP structures. For example, patient-specific tissue scaffolds for bone regeneration requires compressive strength and modulus to at least match those of cancellous bone, which is in the range of 2-20 MPa and 100-2000 MPa, respectively (Røhl *et al.*, 1991; Giesen *et al.*, 2001; Yeni and Fyhrie, 2001; Olszta *et al.*, 2007; Fu *et al.*, 2011). However, the 3D printed bioceramic scaffolds developed in most previous studies have insufficient mechanical properties to meet the requirement for bone

tissue engineering applications (Chumnanklan *et al.*, 2007; Gbureck *et al.*, 2008; Szucs and Brabazon, 2008; Zhou *et al.*, 2012). Weak bonding can subsequently compromise other properties, such as barrier properties, and long-term structural integrity under humid or physiological environments. The authors have previously demonstrated that CaSO<sub>4</sub> porous structures manufactured using 3DP technology completely disintegrated within 7 days when immersed in pH=7.4 buffer solution (Zhou *et al.*, 2012). Coupled with insufficient mechanical stability, this results in an inability to support surrounding tissue in a load-bearing site.

To address this challenge, different approaches have been used to enhance mechanical performances of 3DP tissue engineered bone scaffolds. Many studies have focused on the selection of different liquid binders to increase powder-binder reactivity (Peters *et al.*, 2006; Gbureck *et al.*, 2007; Vorndran *et al.*, 2008). Vorndran *et al.* (2008) compared the quality of 3DP scaffolds (in this case calcium phosphate) using water-based and acid binders, which offered different compressive properties and printing resolution. However, acidic binders cause degradation of the thermal print head used in commercial 3D printers and, in practice, only water-based media (>98% water) can ensure reliable 3DP manufacturing over a sustained period (Rahmati *et al.*, 2009). Another approach was to investigate powder physical and topological properties on a fundamental level (Butcher *et al.*, 2012; Zhou *et al.*, 2014). Powder particle size has been demonstrated to be the most important topological characteristic in affecting powder bed packing, spreadability and wettability. Many studies have investigated powders of various particle size in the 3DP process, which have resulted in different properties of the resultant 3DP structure (Lu *et al.*, 2009; Butcher *et al.*, 2012; Zhou *et al.*, 2014). However, a previous study has reported that even for a highly-packed powder bed, powders only occupied less than 40% of the overall volume within the powder bed, the remaining being occupied by interparticle spacing (Zhou *et al.*, 2014). Sintering has been used to consolidate 3DP ceramic structures to improve their mechanical properties. Due to the coarse particles used in 3DP manufacturing, the rearrangement of particles during sintering is limited and the degree of particle necking is low (Chummanklang *et al.*, 2007). A relatively high shrinkage (18-32%) after sintering has been reported (Seitz *et al.*, 2005; Leukers *et al.*, 2005; Fierz *et al.*, 2008), which requires compensation when considering the original CAD models. Processing parameter optimisation (e.g. layer thickness, build orientation, and binder saturation level) also plays an important role in printing resolution and stability (Patirupanusara *et al.*, 2008; Asadi-Eydivand *et al.*, 2016).

Most of the approaches used to date do not provide solutions to reducing the extent of interparticle spacing within 3DP structures. Consequently, the improvements in mechanical properties have been very limited. A more rational approach to solve this problem would be to focus on filling the interparticle spacing with a binding agent during post-processing for components printed. Normally, 3DP components are immersed in an infiltrant liquid pool to obtain infiltration and also coating on the surface. Commercially available infiltrants for Z-corp 3D printers include wax and epoxy resins. However, to meet demands from an increasing range of businesses, there is a growing imperative to widen the variety of infiltrant that can be used to fill interparticle spacing of 3DP structures. A non-toxic and bioresorbable material would be an attractive proposition for 3DP structures for use in health and safety sectors (e.g. food industry and medical device applications).

Poly ( $\epsilon$ -caprolactone) (PCL) is a bioresorbable polymer that has been commercially used for decades to make implantable medical devices (e.g. Osteopore<sup>TM</sup> and Osteoplug<sup>TM</sup>) (Teoh *et al.*, 2004). It is a biocompatible material and undergoes degradation via hydrolytic cleavage of ester linkages in physiological conditions. PCL provides long-term mechanical stability to withstand forces from both wound contraction and external application owing to its relatively slow resorption profile (Rai *et al.*, 2005). Due to the excellent toughness and processability, PCL is often blended with more brittle materials to improve resistance to stress cracking (Nair and Laurencin, 2007). Coating highly porous ceramics with PCL has been shown to augment compressive properties (Xue *et al.*, 2009 and Zhao *et al.*, 2010). Significant improvements in toughness have also been demonstrated due to the ductile PCL fibrils bridging cracks within brittle ceramics (Peroglio *et al.*, 2007). Due to the bioresorption and toughness, PCL has distinctly different characteristics compared to widely used 3DP ceramic materials, such as CaSO<sub>4</sub>. Therefore, it presents great potential to address the weak bonding within 3DP structures and improve their functions to meet various application requirements.

The aim of this study was to evaluate the effects of adopting PCL coating as a post-process method to augment the performance of 3DP porous structures. Specific properties used to evaluate the extent of improvement were compressive properties, wettability, morphology, and *in vitro* bioresorption. By utilising different parameters during the polymer dip-coating method, (e.g. immersion time, solution concentration, and repeated times) the efficiency of PCL coating and the capability to achieve variable functions of 3DP porous structures was also investigated.

## 2 Materials and Methods

### 2.1 Manufacturing Process

A 3D porous structure was designed with pore size and strut thickness both equal to 1.2 mm. The cylindrical structure had diameter= 13.2 mm and height= 13.2 mm (**Figure 1**). The design was saved in the STL format and then imported to the Zcorp 310 3D printer (Z Corporation, US). Standard CaSO<sub>4</sub> hemihydrate powder (ZP 102, Z Corporation, US) and water-based binder (ZB 7, Z Corporation, US) were used as the base materials for building 3D structures. Layer thickness was 100µm. During the 3DP process, the feed area was first filled with powder and the roller spread a powder layer from the feed area to the build area. The print head deposited binder droplets selectively within the build area. After the first layers were built up, the roller returned to the feed area and then spread another powder layer to the build area. This procedure was repeated continuously until a complete structure was constructed. After the 3DP process, the unbound powder was removed using compressed air. All printed structures were heated in a furnace (BCF 11/8, Elite Thermal System Ltd., UK) at 200 °C for 30 min to dehydrate the CaSO<sub>4</sub> hemihydrate (Zhou *et al.*, 2012).

### 2.2 PCL Coating

PCL coating solution was prepared by dissolving PCL powder (Capa 6506, Perstorp UK Ltd.) in chloroform (288306, Sigma-Aldrich UK) using an ADS-HP1 hotplate stirrer (Asynt Ltd., UK) at a temperature of 22 °C and a stirring speed of 3000 rpm. The dissolution process was defined as complete when all the PCL powder had been dissolved in the solution. 3DP structures were fully immersed in the PCL coating solution. After specific immersion times, each 3DP structure was removed and placed on a grill in the fume cupboard under ambient conditions for 48 h to facilitate solvent evaporation. The mass of each scaffold pre-and post-coating was measured.

Preliminary studies by the authors demonstrated that the maximum saturation for PCL in chloroform was approximately 16 wt.% (data not reported). Consequently, 16 wt.% was selected as the upper limit for PCL concentration investigated in this study. Additional concentration levels below the upper limit were selected at equal intervals. Two recent studies assessed the potential for coating tissue engineered scaffolds using PCL/chloroform

solutions (Zulkifli *et al.*, 2014; Shao *et al.*, 2016). In these studies, 2.5 min and 10 min were used as the immersion times. To investigate the optimum immersion period for scaffolds to be coated with PCL – an extended range of immersion times was selected, which ranged from a relatively short period (30 s) to a prolonged period (30 min) compared to the previous studies (Zulkifli *et al.*, 2014; Shao *et al.*, 2016). The second PCL layer was applied onto each porous structure by repeating the same procedure as described for the first layer. The resultant structure was then heated in the oven at 80 °C for 1 h to help fuse the two layers together (Peroglio *et al.*, 2007). The uncoated, PCL single-layer coated, and PCL double-layer coated porous structures were classified as CaSO<sub>4</sub>, PCL-CaSO<sub>4</sub>, and 2PCL-CaSO<sub>4</sub>.

In summary, the following parameters and levels were considered during the coating procedure:

1. PCL concentration (4, 8, 12, and 16 wt.%);
2. Immersion time (30 s, 5 min, and 30 min);
3. Number of coating layers (single PCL layer and double PCL layers).

### 2.3 Compressive Properties

The compressive properties of each 3DP porous structure was determined using a Universal Materials Test system (EZ50, Lloyds Instruments, UK) with a 1 kN load cell (XLC 01/2419, Lloyds Instruments, UK) and at a rate of displacement of 0.5 mm/min (n = 4). The load cell had a load measurement accuracy of ± 0.5% and could read down to 1/200<sup>th</sup> of its capacity. Each specimen was tested to failure, which was denoted when the load in the post-peak region had reduced to 80% of the peak load. One thousand force-vs.-displacement data points were then logged for each specimen. The compressive strength was defined as the maximum load recorded, divided by the apparent cross-section area (including porosity) of the scaffold. The compressive modulus was determined by measuring the maximum slope of the elastic region of stress-vs.-strain curve immediately after the toe-in region. Simpson's Rule was used to calculate the compressive toughness, which was denoted as the area under the compressive stress-vs.-strain curve to the point of failure. Based on the compressive property data, further characterisation was only conducted on the porous structures that were immersed in 12 wt.% PCL solution for 30 s.

## 2.4 Morphology

3DP structures were also sectioned longitudinally by a blade to facilitate observation of the internal architecture and morphology using field emission SEM (JEOL JSM-6500F, JEOL Ltd., Japan) at an operating voltage of 5 keV. The surfaces of the 3DP structures post-fracture were also analysed using SEM. Each 3DP structure was mounted on aluminium stubs using a cold cure resin (Extec Corp, Enfield, CT 06083-1258, USA), allowed to cure for  $24 \pm 2$  h and subsequently gold-coated using a sputter chamber prior to SEM examination.

## 2.5 Wettability

The surface wettability was investigated by measuring the contact angle of deionised water at room temperature using the sessile drop method (FTA1000B, First Ten Ångstroms, UK). A 5  $\mu$ L droplet of water was placed on the surface at a pump out rate of 2.57  $\mu$ L/s. 3DP structures were sectioned in the longitudinal direction to ensure contact angle measurements were also taken for the internal architecture. A minimum of three specimens were tested from each data set and five readings were performed at different locations on each specimen. Each reading was made by capturing a static contact angle of the sessile drop after a thermodynamic equilibrium was reached between the liquid and the surface. Hydrophilicity was compared between different tested surfaces based on the contact angle results.

## 2.6 *In vitro* Resorption Properties

The resorption properties were determined under pseudo-physiological condition via immersion in tris-HCl buffer solution (pH = 7.4). Each 3DP structure was weighed and then placed in an individual sterile polypropylene 120mL container (Sarstedt AG & Co., Germany) that contained 60mL of tris-HCl buffer solution. Each container was then placed in an oven that was maintained at  $37 \pm 1$  °C (Heraeus® Series 6000, Thermo Fisher Scientific, UK). The resorption properties were measured over a 56 day period. On a weekly basis the buffer solution was replaced with fresh solution. Four 3DP structures were removed from the buffer solution each week; gravimetric analysis and mechanical assessment were conducted. In the first instance, the wet mass was measured after carefully removing all the excess water from the 3DP structure with sterile filter paper. Each 3DP structure was then rinsed with deionised water and dried in a  $37 \pm 1$  °C oven for 48 h. The compressive properties were also determined at each time point after the samples were dried, although determining the compressive properties of the 3DP structures under wet conditions would have been beneficial as this is more representative of in vivo environment. Notwithstanding this fact,



drying each of the 3DP structures prior to mechanical testing was chosen to allow for the non-destructive characterisation to be undertaken beforehand.

The water absorption (%) and mass change (%) before and after immersion in buffer solution were calculated using **Equations 1** and **2**:

$$\% \text{ Water Absorption} = \frac{m_{t,w} - m_{t,d}}{m_{t,d}} \times 100 \quad \text{Equation 1}$$

$$\% \text{ Mass Change} = \frac{m_{0,d} - m_{t,d}}{m_{0,d}} \times 100 \quad \text{Equation 2}$$

Where:  $m_{0,d}$  = dry mass before immersion in buffer solution (g)

$m_{t,w}$  = wet mass after immersion in buffer solution (g)

$m_{t,d}$  = dry mass after immersion in buffer solution (g)

## 2.7 X-ray Microtomography Analysis

X-ray microtomography ( $\mu$ -CT) was used to determine the structural evolution of the 3DP structures in the dry condition as a function of time in tris-HCl buffer solution. At each time point, one 3DP structure was selected for  $\mu$ -CT scanning using a SkyScan 1174 system (SkyScan N.V., Belgium) and scanned at medium resolution (600 axial  $\mu$ -CT slices with  $1024 \times 1024$  pixels bitmap image, 16.25  $\mu$ m resolution). The micro-focus X-ray source operated at a voltage of 50 kV and a current of 800  $\mu$ A. Aluminium filters (0.75 mm) were applied for beam hardening reduction. During the scanning process, the specimen stage was rotated over  $360^\circ$  at rotation step of  $0.5^\circ$ . At each rotation step, an angular shadow projection of the specimen was acquired at an exposure time of 5.5 s. The X-ray shadow projections were then digitised and the acquisition geometry for each scan was extracted from the dataset of transmission images using a reconstruction programme (i.e. smoothing = 4, ring artefact correction = 14 and beam hardening correction = 46%.) The upper and lower threshold levels for reconstructed cross-sectional images were determined from the grayscale histogram, which was generated using ImageJ software (National Institutes of Health, USA). The threshold levels were selected in positions that best separated materials from spaces, as well as one material phase from another if they exhibited distinct peaks within the histogram. Thereafter structural properties of interest (e.g. volume and degree of porosity) were determined using the SkyScan CT-analyser software (Version 1.10.1.0, SkyScan N.V., Belgium).

## 2.8 Statistical Analysis

Data collected from each experimental test was evaluated for statistical significance using SPSS 13.0 software (SPSS, USA). Differences between treatment groups were assessed using one-way Analysis of Variance (ANOVA) with a post-hoc Bonferroni correction. A value of  $p < 0.05$  was considered to be statistically significant. Data analysis was selected on basis of normal probability tests.

## 3 Results

### 3.1 Compressive Properties

Significant improvements ( $p < 0.05$ ) in the compressive properties were achieved after 3DP structures were immersed in the 8, 12, and 16 wt.% PCL solution, compared to the uncoated scaffolds (**Figure 2**). The average compressive strength, modulus and toughness of PCL-CaSO<sub>4</sub> (12 wt.%) increased by 217%, 250%, and 315%, respectively when compared to the uncoated structure. However, no significantly improvements ( $p > 0.05$ ) were demonstrated between the compressive properties for the 3DP structures comprising of PCL-CaSO<sub>4</sub> at 12 wt.% or 16 wt.% concentration.

No significant difference ( $p > 0.05$ ) was observed between the immersion time (0.5, 5 and 30 min) in PCL solution and the resultant compressive properties of the 3DP structures (**Figure 3**). A modest reduction was observed for the compressive strength, modulus and toughness of the 3DP structure immersed in 12 wt.% PCL solution for 30 s ( $3.14 \pm 0.41$  MPa,  $74.13 \pm 8.10$  MPa, and  $0.41 \pm 0.08 \cdot 10^{-6}$  J/m<sup>3</sup>), comparing to 30 min immersion ( $3.28 \pm 0.80$  MPa,  $79.22 \pm 10.00$  MPa, and  $0.50 \pm 0.16 \cdot 10^{-6}$  J/m<sup>3</sup>). Furthermore, there was less than 10% increase in the mass when the immersion time was increased from 30 sec to 5 min or 30 min, which indicated the majority of the PCL coating penetrated the 3DP structure during the initial 30 s of immersion.

Significant differences ( $p < 0.05$ ) in the compressive properties were observed between the 3DP structures as a function of number of coating layers (**Figure 4**). Compressive strength, modulus and toughness increased from  $3.14 \pm 0.31$  MPa,  $74.13 \pm 4.10$  MPa and  $0.41 \pm 0.08 \cdot 10^{-6}$  J/m<sup>3</sup> for a single PCL coating compared to  $5.45 \pm 0.57$  MPa,  $90.1 \pm 7.00$  MPa and  $0.64 \pm 0.10 \cdot 10^{-6}$  J/m<sup>3</sup> for a double PCL coating. Additionally, the average mass increase during first layer coating and second layer coating was 0.166 g and 0.126 g, respectively.

### 3.2 Morphology

SEM images showed significant differences in the surface morphologies between the uncoated and PCL-coated samples (**Figure 5a** and **Figure 5b**). The surface of a 3DP uncoated structure demonstrated a relatively higher degree of roughness and a larger level of visible interparticle spacing. Coating the 3DP structure with PCL filled the interparticle spaces on the surface. Evidence of PCL coating was also observed within the struts of the porous 3DP structures, which was indicative of deep penetration of the PCL coating (**Figure 5d**). Stretched fibrils of PCL containing ceramic particles were noted across the fractured surface of the coated 3DP structures (**Figure 6**).

### 3.3 Surface Hydrophilicity

The water contact angle was determined to evaluate the surface hydrophilicity as a function of PCL coating (**Figure 7**). The surface of 3DP structures manufactured from  $\text{CaSO}_4$  exhibited extreme hydrophilic tendency, immediately imbibing the water droplets once placed on the surface. The water contact angle increased considerably when the PCL coating was applied. However no significant difference ( $p > 0.05$ ) was observed between the application of a single or double layer of PCL to the surface of the 3DP structure. Large variations were observed for the contact angle data when comparing the surfaces of external struts and internal struts of the 3DP porous structures. In contrast the 2PCL- $\text{CaSO}_4$  structure showed more consistent contact angle data. The outer surface of the 3DP structure exhibited higher contact angle when compared to the inner surface irrespective of the number of PCL coating layers applied.

### 3.4 *In vitro* Resorption

The resorption properties of the  $\text{CaSO}_4$  3DP structure changed dramatically on application of the PCL coating. Both PCL- $\text{CaSO}_4$  and 2PCL- $\text{CaSO}_4$  3DP structures were able to maintain the bulk of their shape following 56 days of immersion in buffer solution. The mass gradually reduced as a function of time in buffer solution over the 56-day period (**Figure 8**). A 10% reduction in the original mass was observed for PCL- $\text{CaSO}_4$  and 2PCL- $\text{CaSO}_4$  type structures by Day 7 and by Day 35 this mass reduction was 30%. Beyond Day 42 time point, a significant difference ( $p < 0.05$ ) in the mass change was noted between the PCL- $\text{CaSO}_4$  and 2PCL- $\text{CaSO}_4$  3DP structures.

The extent of water absorption was significantly different ( $p < 0.05$ ) between the PCL- $\text{CaSO}_4$  and 2PCL- $\text{CaSO}_4$  3DP structures during the entire resorption period (**Figure 9**). Following 7

days immersion in buffer solution, the water absorption for the PCL-CaSO<sub>4</sub> structure was 102.20±3.55 % when compared to 67.33±2.03 % for 2PCL-CaSO<sub>4</sub>. At day 56, the water absorption for the PCL-CaSO<sub>4</sub> and 2PCL-CaSO<sub>4</sub> 3DP structures increased further to 261.40±37.76 % and 148.32±10.27 %.

By the end of the resorption study, both the PCL-CaSO<sub>4</sub> and 2PCL-CaSO<sub>4</sub> structures in the dry condition maintained ≤40% of their original compressive strength (**Figure 10a**) and ≤20% of their original compressive modulus (**Figure 10b**). The single layer PCL coated CaSO<sub>4</sub> structure demonstrated a greater reduction in compressive strength when compared to the double PCL coating CaSO<sub>4</sub> structure. At the Day 56 time point, the compressive strength for the PCL-CaSO<sub>4</sub> structure reduced from 3.14±0.31 MPa to 1.38±0.23MPa (-56.05% and the 2PCL-CaSO<sub>4</sub> structure decreased from 5.45±0.57 MPa to 3.07±0.60 MPa (-43.67%). The rate of reduction in compressive modulus was more rapid than the reduction in compressive strength during the initial stages of resorption (i.e. 1-7 days). Thereafter, the compressive modulus for both specimen types decreased at a modest rate until Day 56.

Precipitation of CaSO<sub>4</sub> was more evident following resorption. Precipitation was observed on both the PCL-CaSO<sub>4</sub> and 2PCL-CaSO<sub>4</sub> structures following 7 days immersion in buffer solution (**Figure 11a** and **Figure 11b**). However, by Day 56 the extent of ceramic precipitation disappeared (**Figure 11c**). Ceramic particles were still evident following 56 days in buffer solution, which were encased within the PCL coating. The surface morphology of the PCL coated structures did not seem to alter over the resorption period of 56 days (**Figure 11d**).

### 3.5 $\mu$ -CT Analysis

One of the challenges of analysing changes in the structural properties as a function of resorption time was the continuous shift in the X-ray absorption peaks on the grayscale histogram, which was due to changes in the density of the specimen. To determine the optimum threshold levels that could be applied on a continuous basis, the grayscale histograms for specimens taken at Day 0 to Day 56 were analysed in parallel. In this study, the X-ray absorption peaks shifted between different time points. The PCL-CaSO<sub>4</sub> (Day 0) exhibited the X-ray absorption peak in a grayscale range of 40 and 120 (**Figure 12a**). During Day 7 and Day 21, the X-ray absorption peak shifted towards the higher grayscale. However at Day 28 the X-ray absorption peak shifted towards the lower grayscale. The PCL-CaSO<sub>4</sub> 3DP structure exhibited X-ray absorption peaks of between 5 and 25 grayscale from Day 35

to Day 49. No X-ray absorption peak was observed at Day 56. For the 2PCL-CaSO<sub>4</sub> structures, a similar trend was observed (**Figure 12b**). From Day 0 and Day 42, the X-ray absorption characteristic peak shifted between 20 and 140 grayscale. Between Day 49 and Day 56, the 2PCL-CaSO<sub>4</sub> structures exhibited peaks at the lower grayscale range (i.e. 5- 25).

Grayscale values are proportional to the material density (Hawkins *et al.*, 2010). It is postulated that a reduction in material density could be related to the degradation of the 3DP structure as a consequence of resorption time. If the micropore size was smaller than the voxel size of  $\mu$ -CT scanning, then the voxel containing that micropore would still show a grayscale value. Therefore the grayscale value for a voxel was governed by the percentage of empty spaces within that voxel. At the later stages of resorption both the PCL-CaSO<sub>4</sub> and 2PCL-CaSO<sub>4</sub> structures exhibited distinct X-ray absorption peaks within the low grayscale range (5-25), which was indicative of a low density due to a relatively higher level of resorption. Two threshold levels were subsequently determined: (1) 5 and (2) 25, resulting in three grayscale ranges: (1) 0-5, (2) 5-25, and (3) 25-255 (Table 1). Voxels carrying grayscale of 5-25 and 25-255 were considered as low-density and high-density materials. The grayscale range of 0-5 corresponded to the empty space.

Different binary images were obtained after using different thresholding levels (**Table 2**). A small percentage of material was observed between the 5 and 25 grayscale range at Day 0 and Day 7, which could only be observed on the surface. Below the surface, all material was in the grayscale range of between 25 and 255. The binary images of 2PCL-CaSO<sub>4</sub> did not exhibit great changes at Day 28. However, some material within the internal structure of PCL-CaSO<sub>4</sub> changed to a lower grayscale range (5-25). The majority of the internal structure for the PCL-CaSO<sub>4</sub> and 2PCL-CaSO<sub>4</sub> converted into the lower grayscale range (5-25) by Day 56 and only the outer layers of the 3DP structure remained in the upper grayscale range (25-255).

PCL-CaSO<sub>4</sub> had an overall volume of 898.47 mm<sup>3</sup> prior to immersion in the buffer solution and most of the structure was within the 25-255 grayscale range (**Figure 13a**). The overall volume of the material gradually decreased to 699.07 mm<sup>3</sup> by Day 49. The volume ratio of high-density materials to low-density materials also reduced to  $\geq 1$  at Day 49, which indicated the majority of material was within the 5-25 grayscale range. A greater reduction in the overall volume of the 3DP structure was observed from Day 49 to Day 56. In contrast, the 2PCL-CaSO<sub>4</sub> structures did not demonstrate a large decrease in the overall volume of

material (**Figure 13b**). However, a continuous reduction in the volume ratio of high-density materials to low-density materials was also observed between Day 0 (6.41) and Day 56 (0.49).

For PCL-CaSO<sub>4</sub>, the percentage of spaces increased gradually from 37.44% (Day 0) to 49.95% (day 49) (**Figure 14**). An additional significant rise was observed from Day 49 to Day 56 (69.34%), which concurred with the overall material volume reduction. The percentage of space increased gradually from 37.44% (Day 0) to 58.8% (Day 28) for the 2PCL-CaSO<sub>4</sub> structures. No distinct change in percentage of space was evident beyond Day 28.

## 4 Discussion

To investigate the effects of PCL coating on 3DP structures, it is more logical to perform the study using a well-established material for this technology. Many materials such as hydroxyapatite still require more thorough investigations to the most efficient and reliable binding approach as well as to optimise powder physical and topological properties. CaSO<sub>4</sub> has been the dominant material for manufacturing 3DP structure since the emergence of the technology. Historically, the CaSO<sub>4</sub> based material has been successfully used as a biocompatible material to substitute bone tissues for regeneration (Peltier *et al.*, 1957). Unlike other approaches attempting to optimise physical or chemical properties of processed materials, PCL coating aims directly to address the inherent drawback on the morphology of a 3DP structure. Therefore, it is highly applicable to different materials processed using 3DP technology and justifies the use of CaSO<sub>4</sub> powdered material in this study. The outcome from this study can be used as a guideline for application to other powdered formulations processed using 3DP technology.

Post-processing of 3DP structures has been strongly advocated in an effort to augment the mechanical properties (Butscher *et al.*, 2011). In this regard, a polymer dip-coating method was utilised to apply a PCL coating onto the 3DP structure. It was hypothesised that PCL would provide additional strength and toughness to the brittle CaSO<sub>4</sub> material. The compressive properties of the 3DP structure increased considerably on application of the PCL coating. Under compression loading, fracture was normally initiated at the weakest points within the 3DP structure, i.e. the bonded area between adjacent powders containing surface flaws and gaps. Following evaporation of the solvent, the PCL coating adhered to the CaSO<sub>4</sub>

particles (**Figure 15**). The layer of PCL coating covered these surface flaws and filled the interparticle spacing, which strengthened the bond between the CaSO<sub>4</sub> particles. In this study, SEM analysis clearly demonstrated the PCL coating filled the interparticle spacing between the CaSO<sub>4</sub> particles.

PCL offers good toughness when compared to most other bioresorbable polymers (Roohani-Esfahani *et al.*, 2010), which contributed to improvements in the compressive properties of 3DP structures. When the load exceeded the capacity of the brittle ceramic material, the stress was distributed to PCL layers and the energy was absorbed by the PCL coating. It has been reported that PCL can reach 7% and 80% elongation at yield and break point respectively (Agrawal and Ray, 2001; Shor *et al.*, 2007). In this study PCL-CaSO<sub>4</sub> underwent severe deformation under compression; however there was no evidence of fracture within the 3DP structure. The PCL-CaSO<sub>4</sub> 3DP structure maintained its overall shape post-failure, while the uncoated equivalent failed catastrophically. SEM analysis of the fractured surfaces from the PCL-CaSO<sub>4</sub> showed evidence of crack bridging by the PCL fibrils, which confirmed the role of PCL coating in augmentation of the mechanical properties.

Improvements in mechanical properties were also influenced by the coating concentration and the number of coating layers. Increasing the PCL concentration up to 12 wt.% offered a greater adherence throughout the 3DP structure. Consequently the overall structure was further reinforced, thereby increasing the mechanical properties. The PCL solution at 16 wt.% was found difficult to prepare, it is suggested this concentration level exceeded PCL saturation in the solvent. The molecular weight of PCL is one of the properties that may affect the concentration. It is easier to dissolve and infiltrate using PCL of lower molecular weight. However, it would compromise the improvement of toughness to the 3DP structures. Additionally the duration of the immersion time in the PCL solution beyond 30 s did not offer further improvement in the mechanical properties. Application of a double layer of PCL coating achieved both a higher degree of coverage and a greater quantity of PCL material over the surface of the 3DP structure. Consequently a step-change improvement in the compressive properties was observed for the 2PCL-CaSO<sub>4</sub> structures.

PCL is known for slow resorption due to its hydrophobicity and highly crystalline structure (Khan *et al.*, 2013). In this study, the uncoated 3DP structures disintegrated within a week, while only 10% mass loss was recorded for PCL-coated samples following 7 day immersion in buffer solution. The disintegration of the CaSO<sub>4</sub> 3DP structure in the buffer solution was

due to dimensional expansion and the dissolution therein. The layers of PCL coating provided protection to the CaSO<sub>4</sub> particles from exposure to water molecules, as well as maintaining the structural integrity of the 3DP component.

PCL undergoes hydrolytic cleavage of ester linkages during the first 12 months of resorption before its molecular weight reduced to a low enough level for resorption (Sun *et al.*, 2009). Therefore, a limitation of this study was to conduct a resorption experiment over a 56-day period. Notwithstanding this fact, both PCL coated 3DP structures demonstrated a reduction of almost 50% of their original mass by Day 56. Considering the high dissolution rate of CaSO<sub>4</sub>, it can be suggested the coating material played a crucial role in determining the resorption behaviour of the composite.

Even though PCL-CaSO<sub>4</sub> demonstrated lower PCL coverage when compared to the 2PCL-CaSO<sub>4</sub> structures - no significant difference ( $p>0.05$ ) in the resorption properties was observed until Day 49. The comparable resorption profile could be due to the accumulation of Ca<sup>2+</sup> and SO<sub>4</sub><sup>2-</sup> ions within some regional areas, which would cause oversaturation of ions and dissolution by-products making further dissolution difficult.

Water absorption is influenced by the water uptake of the residual material and the number of surface micropores that can trap water (Yang *et al.*, 2008). PCL-CaSO<sub>4</sub> demonstrated a significantly higher water absorption ( $p<0.05$ ) when compared to the 2PCL-CaSO<sub>4</sub>. Different distributions with respect to surface hydrophilicity were observed for the 3DP structures coated with single and double layers of PCL coating, which was due to the lower surface coverage for PCL-CaSO<sub>4</sub> and consequently more surface micropores and flaws being exposed to the buffer solution.

The compressive properties of the coated 3DP structures were governed by the more rigid PCL material. When CaSO<sub>4</sub> particles dissolved, the proportion of PCL within the composite increased and therefore enhanced its role in determining the overall mechanical properties. This observation was more significant for 2PCL-CaSO<sub>4</sub>, which had more PCL material within the composite than the PCL-CaSO<sub>4</sub> structures. Consequently the polymer within the 2PCL-CaSO<sub>4</sub> structure offered greater support to the CaSO<sub>4</sub> fused particles when subjected to compressive loading.

Materials undergoing resorption experience variations in density when compared to the control. The X-ray absorption peaks shifted significantly over the 56-day period and a



grayscale range of 5 to 25 grayscale was observed at the latter stages of resorption for both PCL-CaSO<sub>4</sub> and 2PCL-CaSO<sub>4</sub> structures. This grayscale range represented material that was resorbed extensively to a relatively low density. Such an interesting finding offered an opportunity to segment the  $\mu$ -CT data into two distinct material phases: (1) high-density material representing a slight resorbable class and (2) low-density material representing a higher resorbable class.

The overall volume of material (grayscale range: 5-255) corresponded well with the gravimetric data for both the PCL-CaSO<sub>4</sub> and 2PCL-CaSO<sub>4</sub> structures as a function of immersion time. A more rapid reduction in the overall material volume occurred at Day 56 for PCL-CaSO<sub>4</sub>, which coincided with the trends observed for the mass loss data. The proportion of materials within grayscale range of 5-25 increased significantly for PCL-CaSO<sub>4</sub> as a function of resorption time, which explains the reduction in compressive properties. Once the material had resorbed, pores were created within the same location. According to the  $\mu$ -CT data, the porosity increase for the 3DP structures corresponded to an increase in material loss. The rate of increase in the overall porosity (grayscale range: 5-255) was slow and only a rapid increase occurred at Day 56 for the PCL-CaSO<sub>4</sub>, which paralleled well with the material volume.

In this study, the mechanism of the polymeric addition could be considered both a coating and an infiltrate. Specific reasons for this consideration include: (1) the external and internal surfaces of scaffolds were largely covered by PCL; and (2) the PCL also infiltrated the interparticle spacing between adjacent powder particles within the 3DP printed structures (Figure 5). There may be some concerns of pore blockage as a consequence of polymer infiltration. However in this study this is not the case, the PCL coating did not occlude any of the pores within the printed structure. Application of the PCL coating reduced the extent of the interparticle spacing within the printed structure and assisted in overcoming one of the main drawbacks of 3DP technology.

A potential limitation of this study was the choice of a relatively large pore size for the printed structures. However, it has been reported that trabecular bone demonstrates an average pore size of 500-1500  $\mu$ m and a porosity of 50% - 90% (Cowin, 2001). A minimum pore size of 1.2 mm was chosen based on a previous study conducted by the authors, whereby they investigated the manufacturability of CaSO<sub>4</sub> 3DP structures of differing pore size and strut configurations (Zhou *et al.*, 2012). They reported it was extremely difficult to remove

the unbound CaSO<sub>4</sub> powder particles from the 3DP structures when a pore size of less than 0.8 mm was used. The relationship between scaffold pore size and cellular activity within tissue engineered scaffolds is not fully understood as is apparent from the conflicting reports on the optimal pore size found within the literature. Scaffolds with mean pore sizes ranging from 20 µm to 1500 µm have been used in bone tissue engineering applications (Pilliar *et al.*, 1986; Nehrer *et al.*, 1997; Baksh *et al.*, 1998; Lee *et al.*, 2004; Williams *et al.*, 2005). Early studies using porous implants demonstrated that the minimum pore size for significant bone growth was 75–100 µm with an optimal range of 100–350 µm for load bearing applications (Hulbert *et al.*, 1970; Klawitter and Hulbert, 1971; Klawitter *et al.*, 1976). Since this work many studies have proposed a need for pores exceeding 650 µm for bone formation, to ensure rapid vascularisation and for the survival of transplanted cells within tissue engineered scaffolds constructs. By facilitating capillary formation, pores greater than 650 µm can lead to direct osteogenesis while pores smaller than 300 µm have the potential to promote osteochondral ossification (Tsuruga *et al.*, 1997; Cornell, 1999; Kuboki *et al.*, 2001; Götz *et al.*, 2004; Karageorgiou *et al.*, 2005; Lien *et al.*, 2009; Roosa *et al.*, 2010). However, it is important to identify the upper limits in pore size as large pores may compromise the mechanical properties of the scaffolds by increasing void volume (Karageorgiou *et al.*, 2005).

There are also potential drawbacks associated with polymer coating, such as compromising osteoconductivity of a bioceramic surface and cytotoxicity of residual solvent. It is suggested that more ‘friendly’ solvent, such as scCO<sub>2</sub>, should be considered to utilise in future studies. Nevertheless, the focus of this study was to evaluate the use of PCL coating as a highly effective approach to addressing the main limitations of current 3DP manufacturing. And it has successfully filled the interparticle voids within 3DP structures and consequently improved various key performances. The outcome of this study contributes to the continuous development of powder-based 3DP technology increasing the robustness of manufactured products creating opportunities to increase their applications.

## 5 Conclusion

The overall performance of 3DP ceramic structures improved through the application of PCL coating. Adoption of PCL coating technology as a post-processing option has been demonstrated as a highly efficacious method of reducing the **interparticle spacing** and altering surface properties of 3DP structures. The surface morphology, microstructure and

hydrophilicity of 3DP components were subsequently modified, which augmented the compressive properties and *in vitro* resorption behaviour. The average compressive strength, Young's modulus, and toughness increased 217%, 250%, and 315%, following PCL coating. PCL coating has successfully increased the compressive properties of 3DP porous structures to the lower limit of the range of those of cancellous bones. Additionally, the overall structural integrity of the 3DP structure was maintained for up to 56 days in buffer solution as the PCL coating inhibited the rapid dissolution of CaSO<sub>4</sub> particles. The  $\mu$ -CT data indicated the resorption behavior was predominantly related to microstructural conversion from high density to low density material, as opposed to a significant reduction in material volume. Therefore, the PCL coated bioceramic structure could provide mechanical support to the surrounding tissues without failing prematurely *in vivo*.

The coating method also demonstrated a high degree of flexibility and the properties of 3DP structures could be further tailored by using different coating parameters. Introduction of a second layer of coating and using a solution with an increased PCL concentration facilitated a higher degree of surface coverage and depth of penetration of the PCL coating. In addition, the extent of PCL coating could be controlled by using solutions with different PCL concentrations. The release rate of ceramic material into environment was controlled by the surface coverage of PCL. Overall, the PCL coated bioceramic structures developed present compressive and bioresorbable properties applicable within the field of tissue engineered bone substitutes.

## REFERENCES

- AGRAWAL, C. and RAY, R.B., 2001. Biodegradable polymeric scaffolds for musculoskeletal tissue engineering. *Journal of Biomedical Materials Research*, 55(2), pp. 141-150.
- ASADI-EYDIVAND, M., SOLATI-HASHJIN, M., FARZAD, A. and OSMAN, N.A.A., 2016. Effect of technical parameters on porous structure and strength of 3D printed calcium sulfate prototypes. *Robotics and Computer-Integrated Manufacturing*, 37, pp. 57-67.
- BAKSH, D., DAVIES, J.E. and KIM, S., 1998. Three-dimensional matrices of calcium polyphosphates support bone growth *in vitro* and *in vivo*. *Journal of Materials Science: Materials in Medicine*, 9, pp. 743-748.
- BUTSCHER, A., BOHNER, M., HOFMANN, S., GAUCKLER, L. and MÜLLER, R., 2011. Structural and material approaches to bone tissue engineering in powder-based three-dimensional printing. *Acta Biomaterialia*, 7(3), pp. 907-920.
- BUTSCHER, A., BOHNER, M., ROTH, C., ERNSTBERGER, A., HEUBERGER, R., DOEBELIN, N., RUDOLF VON ROHR, P. and MÜLLER, R., 2012. Printability of calcium phosphate powders for three-dimensional printing of tissue engineering scaffolds. *Acta Biomaterialia*, 8(1), pp. 373-385.
- CHIA, H.N. and WU, B.M., 2015. High-resolution direct 3D printed PLGA scaffolds: print and shrink. *Biofabrication*, 7(1), pp. 015002.
- CHUMNANKLANG, R., PANYATHANMAPORN, T., SITTHISERIPRATIP, K. and SUWANPRATEEB, J., 2007. 3D printing of hydroxyapatite: Effect of binder concentration in pre-coated particle on part strength. *Materials Science and Engineering: C*, 27(4), pp. 914-921.
- CORNELL, C.N., 1999. Osteoconductive materials and their role as substitutes for autogenous bone grafts. *Orthopaedic Clinics of North America*, 30(4), pp. 591-598.
- COWIN, S.C., 2001. Bone Mechanics Handbook. volume 1, CRC Press, Boca Raton, Fla, USA, 2<sup>nd</sup> edition, 2001.
- D'AVENI, R.A., 2013. 3-D printing will change the world. *Harvard business review*, 91(3), pp. 34-35.
- FIERZ, F.C., BECKMANN, F., HUSER, M., IRSEN, S.H., LEUKERS, B., WITTE, F., DEGISTIRICI, Ö., ANDRONACHE, A., THIE, M. and MÜLLER, B., 2008. The morphology of anisotropic 3D-printed hydroxyapatite scaffolds. *Biomaterials*, 29(28), pp. 3799-3806.
- FU, G., SAIZ E., RAHAMAN, M.N. and TOMSIA, A.P., 2011. Bioactive glass scaffolds for bone tissue engineering: State of the art and future perspectives. *Materials Science and Engineering: C*, 31, pp. 1245-1256.
- GBURECK, U., VORNDRAN, E., MÜLLER, F.A. and BARRALET, J.E., 2007. Low temperature direct 3D printed bioceramics and biocomposites as drug release matrices. *Journal of Controlled Release*, 122(2), pp. 173-180.

- GIESEN, E.B., DING, M., DALSTRA, M. and VAN EIJDEN, T.M., 2001. Mechanical properties of cancellous bone in the human mandibular condyle are anisotropic. *Journal of Biomechanics*, 34, pp. 799-803.
- GÖTZ, H., MÜLLER, M., EMMEL, A., HOLZWARTH, U., ERBEN, R. and STANGL, R., 2004. Effect of surface finish on the osseointegration of laser-treated titanium alloy implants. *Biomaterials*, 25(18), pp. 4057-4064.
- HAWKINS, J., CIFUENTES, M., PLESHKO, N.L., AMBIA-SOBHAN, H. and SHAPSES, S.A., 2010. Energy restriction is associated with lower bone mineral density of the tibia and femur in lean but not obese female rats. *Journal of Nutrition*, 140(1), pp. 31-37.
- HULBERT, S.F., YOUNG, F.A., MATHEWS, R.S., KLAWITTER, J.J., TALBERT, C.D. and STELLING, F.H., 1970. Potential of ceramic materials as permanently implantable skeletal prostheses. *Journal of Biomedical Materials Research*, 4, pp. 433-456.
- HUSON, D. and HOSKINS, S., 2014. 3D Printed Ceramics for Tableware, Artists/Designers and Specialist Applications, *Key Engineering Materials* 2014, Trans Tech Publ, pp. 351-357.
- ILIESCU, M., TABESHFAR, K., IGHIGEANU, A. and DOBRESCU, G., 2009. Importance of rapid prototyping to product design. *UPB Sci.Bull., Series D*, 71(2), pp. 117-125.
- KARAGEORGIU, V. and KAPLAN, D., 2005. Porosity of 3D biomaterial scaffolds and osteogenesis. *Biomaterials*, 26, pp. 5474-5491.
- KHAN, F., VALERE, S., FUHRMANN, S., ARRIGHI, V. and BRADLEY, M., 2013. Synthesis and cellular compatibility of multi-block biodegradable poly ( $\epsilon$ -caprolactone)-based polyurethanes. *J.Mater.Chem.B*, 1(20), pp. 2590-2600.
- KLAWITTER, J.J. and HULBERT, S.F., 1971. Application of porous ceramics for the attachment of load bearing internal orthopaedic applications. *Journal of Biomedical Materials Research*, 5(6), pp. 161-229.
- KLAWITTER, J.J., BAGWELL, J.G., WEINSTEIN, A.M. and SAUER, B.W., 1976. An evaluation of bone growth into porous high density polyethylene. *Journal of Biomedical Materials Research*, 10, pp. 311-323.
- KOLTYGIN, A. and BAZHENOV, V., 2012. Development of a substitute for Z cast molding sand used on installations of 3D printing for obtaining aluminum, magnesium, and iron casting. *Russian Journal of Non-Ferrous Metals*, 53(1), pp. 38-41.
- KUBOKI, Y., JIN, Q. and TAKITA, H., 2001. Geometry of carriers controlling phenotypic expression in BMP-induced osteogenesis and chondrogenesis. *Journal of Bone and Joint Surgery*, 83(90012), pp. S105-S115.
- LAM, C.X.F., MO, X., TEOH, S. and HUTMACHER, D., 2002. Scaffold development using 3D printing with a starch-based polymer. *Materials Science and Engineering: C*, 20(1), pp. 49-56.
- LEE, S.J., LEE, I.W., LEE, Y.M., LEE, H.B. and KHANG, G., 2004. Macroporous biodegradable natural/ synthetic hybrid scaffolds as small intestine submucosa impregnated poly- (D, L-lactide-co-glycolide) for tissue-engineered bone. *Journal of Biomaterials Science, Polymer Education*, 15, pp. 1003-1017.

- LEUKERS, B., GÜLKAN, H., IRSEN, S.H., MILZ, S., TILLE, C., SCHIEKER, M. and SEITZ, H., 2005. Hydroxyapatite scaffolds for bone tissue engineering made by 3D printing. *Journal of Materials Science: Materials in Medicine*, 16(12), pp. 1121-1124.
- LIEN, S., KO, L. and HUANG, T., 2009. Effect of pore size on ECM secretion and cell growth in gelatin scaffold for articular cartilage tissue engineering. *Acta Biomaterialia*, 5(2), pp. 670-679.
- LIM, K., CHEANG, P. and CHANDRASEKARAN, M., 2007. Studies on Porous Titanium Alloy Implant Manufactured by Three Dimensional Solid Freeform Fabrication System, *Advanced Materials Research 2007*, Trans Tech Publ, pp. 107-110.
- LU, K., HISER, M. and WU, W., 2009. Effect of particle size on three dimensional printed mesh structures. *Powder Technology*, 192(2), pp. 178-183.
- NAIR, L.S. and LAURENCIN, C.T., 2007. Biodegradable polymers as biomaterials. *Progress in Polymer Science*, 32(8), pp. 762-798.
- NEHRER, S., BREINAN, H.A., RAMAPPA, A., YOUNG, G., SHORTKROFF, S., LOUIE, L.K., SLEDGE, C.B., YANNAS, I.V. and SPECTOR M., 1997. Matrix collagen type and pore size influence behaviour of seeded canine chondrocytes. *Biomaterials*, 18, pp. 769-776.
- PATIRUPANUSARA, P., SUWANPREUK, W., RUBKUMINTARA, T. and SUWANPRATEEB, J., 2008. Effect of binder content on the material properties of polymethyl methacrylate fabricated by three dimensional printing technique. *Journal of Materials Processing Technology*, 207(1), pp. 40-45.
- PELTIER, L.F., BICKEL, E.Y., LILLO, R. and THEIN, M.S., 1957. The use of plaster of Paris to fill defects in bone. *Annals of Surgery*, 146(1), pp. 61.
- PEROGLIO, M., GREMILLARD, L., CHEVALIER, J., CHAZEAU, L., GAUTHIER, C. and HAMAIDE, T., 2007. Toughening of bio-ceramics scaffolds by polymer coating. *Journal of the European Ceramic Society*, 27(7), pp. 2679-2685.
- PETERS, F., GROISMAN, D., DAVIDS, R., HÄNEL, T., DÜRR, H. and KLEIN, M., 2006. Comparative Study of patient individual implants from  $\beta$ -tricalcium phosphate made by different techniques based on CT data. *Materialwissenschaft und Werkstofftechnik*, 37(6), pp. 457-461.
- PILLIAR, R.M., LEE, J.M. and MANIATOPOULOS, C., 1986. Observations on the effect of movement on bone ingrowth into porous-surfaced implants. *Clinical Orthopaedics and Related Research*, pp. 108-113.
- RAHMATI, S., SHIRAZI, F. and BAGHAYERI, H., 2009. Perusing Piezoelectric Head Performance in a New 3-D Printing Design. *Tsinghua Science & Technology*, 14, pp. 24-28.
- RAI, B., TEOH, S., HUTMACHER, D., CAO, T. and HO, K., 2005. Novel PCL-based honeycomb scaffolds as drug delivery systems for rhBMP-2. *Biomaterials*, 26(17), pp. 3739-3748.

ROOHANI-ESFAHANI, S., LU, Z. and ZREIQAT, H., 2011. Novel, simple and reproducible method for preparation of composite hierarchical porous structure scaffolds. *Materials Letters*, 65(17), pp. 2578-2581.

ROOSA, S.M., KEMPPAINEN, J.M., MOFFITT, E.N., KREBSBACH, P.H. and HOLLISTER, S.J., 2010. The pore size of polycaprolactone scaffolds has limited influence on bone regeneration in an *in vivo* model. *Journal of Biomedical Materials Research A*, 92(1), pp. 359-368.

OLSZTA, M.J., CHENG, X., JEE, S.S. KUMAR, R., KIM, Y.Y., KAUFMAN, M.J., DOUGLAS, E.P. and GOWER, L.B., 2007. Bone Structure and Formation: a New Perspective. *Material Science and Engineering: R: Reports*, 58(3), pp. 77-116.

SAIDIN, W., WAGIMAN, A. and IBRAHIM, M., 2013. Development of Wood-Based Composites Material for 3D Printing Process, *Applied Mechanics and Materials* 2013, Trans Tech Publ, pp. 987-991.

SEITZ, H., RIEDER, W., IRSEN, S., LEUKERS, B. and TILLE, C., 2005. Three-dimensional printing of porous ceramic scaffolds for bone tissue engineering. *Journal of Biomedical Materials Research Part B: Applied Biomaterials*, 74(2), pp. 782-788.

SHAO, H., HE, Y., FU, J., HE, D., YANG, X., XIE, J., YAO, C., YE, J., XU, S. and GOU, Z., 2016. 3D printing magnesium-doped wollastonite/ $\beta$ -TCP bioceramics scaffolds with high strength and adjustable degradation. *Journal of the European Ceramic Society*, 36(6), pp. 1495-1503.

SHIRAZI, S.F.S., GHAREHKHANI, S., MEHRALI, M., YARMAND, H., METSELAAR, H.S.C., KADRI, N.A. and OSMAN, N.A.A., 2015. A review on powder-based additive manufacturing for tissue engineering: selective laser sintering and inkjet 3D printing. *Science and Technology of Advanced Materials*, 16(3), pp. 033502.

SHOR, L., GÜÇERİ, S., WEN, X., GANDHI, M. and SUN, W., 2007. Fabrication of three-dimensional polycaprolactone/hydroxyapatite tissue scaffolds and osteoblast-scaffold interactions *in vitro*. *Biomaterials*, 28(35), pp. 5291-5297.

SINGH, N. and MIDDENDORF, B., 2007. Calcium sulphate hemihydrate hydration leading to gypsum crystallization. *Progress in Crystal Growth and Characterization of Materials*, 53(1), pp. 57-77.

SUN, H., MEI, L., SONG, C., CUI, X. and WANG, P., 2006. The *in vivo* degradation, absorption and excretion of PCL-based implant. *Biomaterials*, 27(9), pp. 1735-1740.

TEOH, S.H., TAN, K.C., HUTMACHER, D., LIM, T.C., SCHANTZ, J. and CHOU, N., 2004. Bioabsorbable plug implants and method for bone tissue regeneration. *U.S. Patent Application*, 10/579,946.

TSURUGA, E., TAKITA, H., ITOH, H., WAKISAKA, Y. and KUBOKI, Y., 1997. Pore size of porous hydroxyapatite as the cell-substratum controls BMP-induced osteogenesis. *Journal of Biochemistry*, 121(2), pp. 317-324.

XUE, W., BANDYOPADHYAY, A. and BOSE, S., 2009. Polycaprolactone coated porous tricalcium phosphate scaffolds for controlled release of protein for tissue engineering. *Journal of Biomedical Materials Research Part B: Applied Biomaterials*, 91(2), pp. 831-838.

- YANG, Y., ZHAO, Y., TANG, G., LI, H., YUAN, X. and FAN, Y., 2008. *In vitro* degradation of porous poly (l-lactide-co-glycolide)/ $\beta$ -tricalcium phosphate (PLGA/ $\beta$ -TCP) scaffolds under dynamic and static conditions. *Polymer Degradation and Stability*, 93(10), pp. 1838-1845.
- YENI, Y.N. and FYHRIE, D.P., 2001. Finite element calculated uniaxial apparent stiffness is a consistent predictor of uniaxial apparent strength in human vertebral cancellous bone tested with different boundary conditions. *Journal of Biomechanics*, 34, pp. 1649-1654.
- VORNDRAN, E., KLARNER, M., KLAMMERT, U., GROVER, L.M., PATEL, S., BARRALET, J.E. and GBURECK, U., 2008. 3D Powder Printing of  $\beta$ -Tricalcium Phosphate Ceramics Using Different Strategies. *Advanced Engineering Materials*, 10(12), pp. B67-B71.
- WILL, J., MELCHER, R., TREUL, C., TRAVITZKY, N., KNESER, U., POLYKANDRIOTIS, E., HORCH, R. and GREIL, P., 2008. Porous ceramic bone scaffolds for vascularized bone tissue regeneration. *Journal of Materials Science: Materials in Medicine*, 19(8), pp. 2781-2790.
- WILLIAMS, J.M., ADEWUNMI, A., SCHEK, R.M., FLANAGAN, C.L., KREBSBACH, P.H., FEINBERG, S.E., HOLLISTER, S.J. and DAS, S., 2005. Bone tissue engineering using polycaprolactone scaffolds fabricated via selective laser sintering. *Biomaterials*, 26, pp. 4817-4827.
- WILLIAMS, C.B. and ROSEN, D.W., 2007. Manufacturing Metallic Parts with Designed Mesostructure via Three-Dimensional Printing of Metal Oxide Powder. *Solid Freeform Fabrication Symposium 2007*, pp. 586-596.
- ZHAO, J., GUO, L., YANG, X. and WENG, J., 2008. Preparation of bioactive porous HA/PCL composite scaffolds. *Applied Surface Science*, 255(5), pp. 2942-2946.
- ZHOU, Z., BUCHANAN, F. MITCHELL, C.A. and DUNNE, N., 2012. Effects of Heat Treatment on the Mechanical and Degradation Properties of 3D-Printed Calcium-Sulphate-Based Scaffolds. *ISRN Biomaterials*, Volume 2013, 10 Pages.
- ZHOU, Z., BUCHANAN, F., MITCHELL, C.A., and DUNNE, N., 2014. Printability of Calcium Phosphate:Calcium Sulphate Powders for the Application of Tissue Engineered Bone Scaffolds using the 3D Printing Technique. *Materials Science and Engineering C*, 38, pp. 1-10.
- ZHOU, Z., BUCHANAN, F., LENNON, A. and DUNNE, N., 2015. Investigating Approaches for Three-Dimensional Printing of Hydroxyapatite Scaffolds for Bone Regeneration. *Key Engineering Materials*, 631, pp. 306-311.
- ZULKIFLI, F.H., HUSSAIN, F.S.J., RASAD, M.S.B.A. and YUSOFF, M.M., 2014. *In vitro* degradation study of novel HEC/PVA/collagen nanofibrous scaffold for skin tissue engineering applications. *Polymer Degradation and Stability*, 110, pp. 473-481.



## FIGURES

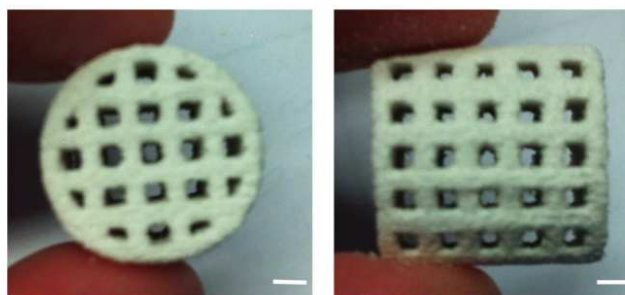


**Fig. 1 – Top view (left) and side view (right) of a scaffold printed. Scale bar=2 mm.**

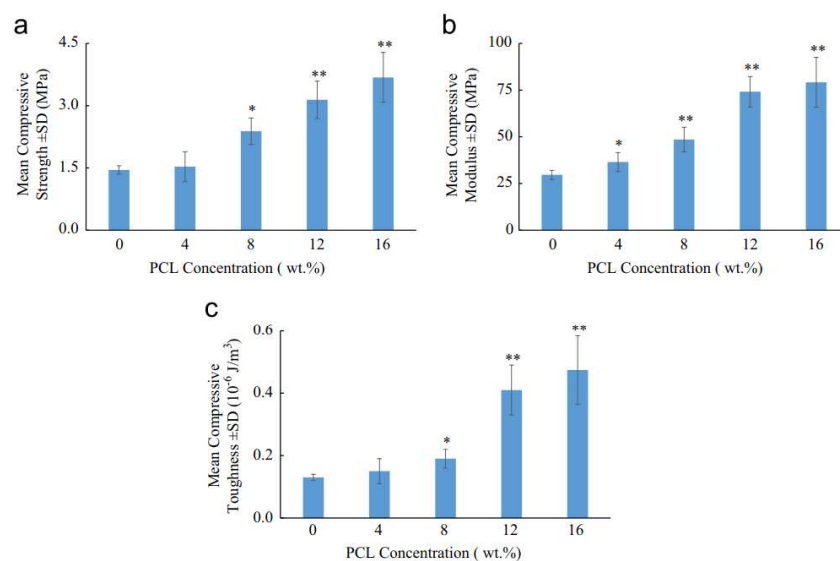


**Fig. 2 – (a) Compressive strength, (b) compressive modulus, and (c) compressive toughness (Mean  $\pm$  SD) for PCL-CaSO<sub>4</sub> samples immersed in PCL solution for 30 s at different PCL concentrations. \* P-value < 0.05 and \*\* P-value < 0.001, indicating a significant difference between control and PCL-CaSO<sub>4</sub> sample.**

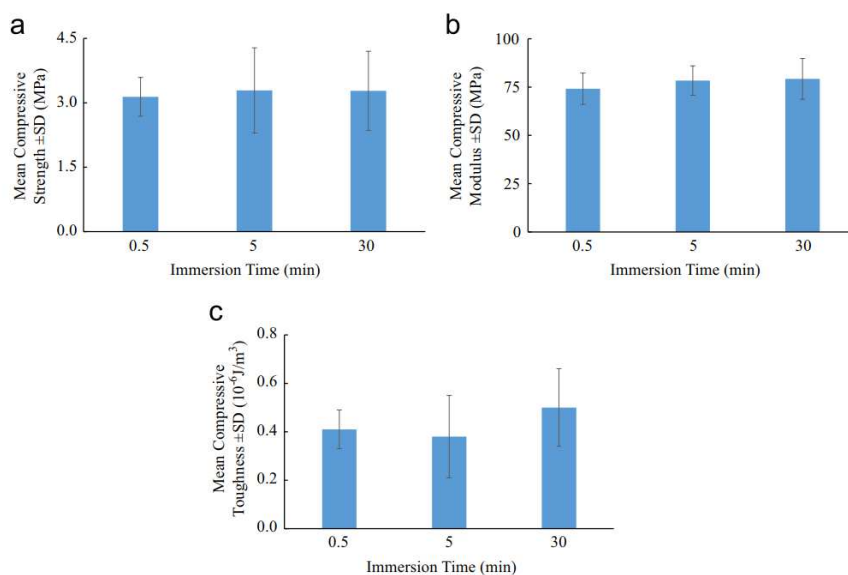


**Fig. 3 – (a) Compressive strength, (b) compressive modulus, and (c) compressive toughness (Mean  $\pm$  SD) for PCL-CaSO<sub>4</sub> samples immersed in 12 wt% PCL solution for different durations.**

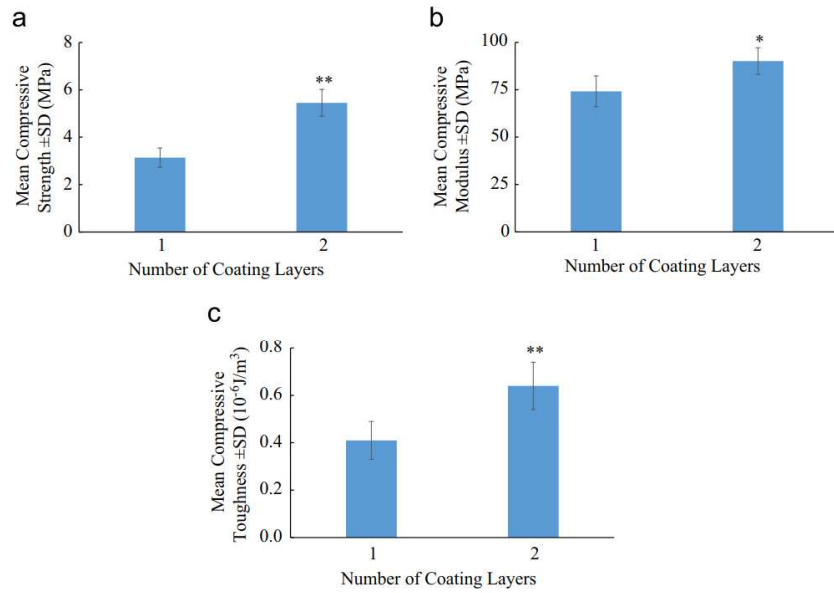


Fig. 4 – (a) Compressive strength, (b) compressive modulus, and (c) compressive toughness (Mean  $\pm$  SD) for PCL-CaSO<sub>4</sub> and 2PCL-CaSO<sub>4</sub> samples. Both scaffolds had been immersed in 12 wt% PCL solution for 30 s. \* P-value < 0.05 and \*\* P-value < 0.001, indicating a significant difference between PCL-CaSO<sub>4</sub> and 2PCL-CaSO<sub>4</sub> samples.

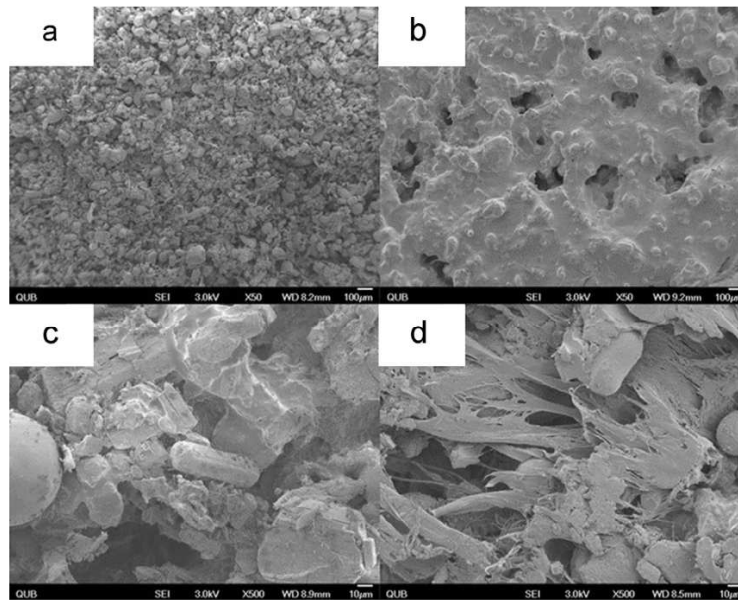


Fig. 5 – SEM images of the (a) surface of an uncoated CaSO<sub>4</sub> (50  $\times$ ); (b) surface of a PCL-CaSO<sub>4</sub> (50  $\times$ ); (c) cross section of an uncoated CaSO<sub>4</sub> (500  $\times$ ); (d) cross section of the inner structure of a PCL-CaSO<sub>4</sub> (500  $\times$ ).

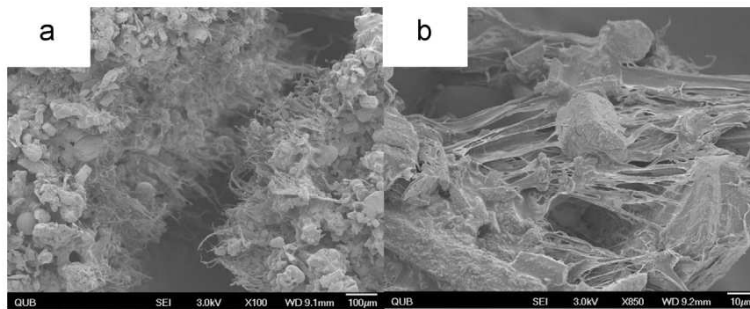


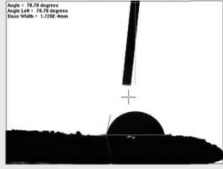


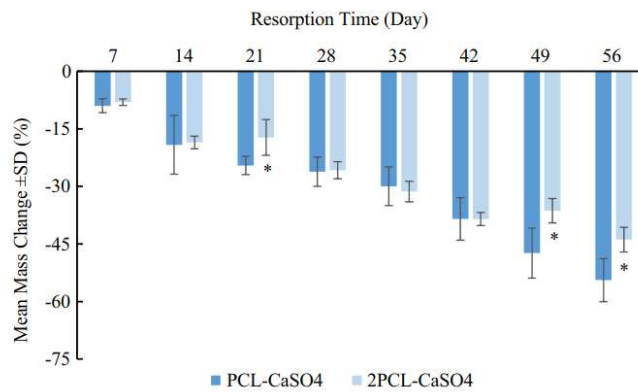


Fig. 6 – SEM images of the (a) fracture surface of a PCL-CaSO<sub>4</sub> (100  $\times$ ); and (b) PCL fibrils connecting CaSO<sub>4</sub> particles in the fracture surface (850  $\times$ ).

| Outer Surface   |   |  |
|---|---|--|
| Uncoated CaSO <sub>4</sub>  | PCL-CaSO <sub>4</sub>   | 2PCL-CaSO <sub>4</sub>   |
|  |  |  |
| 0°  | 43.08 ± 11.75°  | 57.34 ± 3.10°  |
| Inner Surface   |   |  |
|   |  |  |
| N/A   | 29.83 ± 17.35°  | 43.01 ± 7.93°  |

**Fig. 7** – Water contact angles (Mean ± SD) of CaSO<sub>4</sub>, PCL-CaSO<sub>4</sub> and PCL-2CaSO<sub>4</sub> surfaces. Both inner and outer surfaces were tested for PCL-coated samples.



**Fig. 8** – Mass changes (Mean ± SD) for PCL-CaSO<sub>4</sub> and 2PCL-CaSO<sub>4</sub> scaffolds following resorption up to 56 days. \* P-value < 0.05 indicating a significant difference between PCL-CaSO<sub>4</sub> and 2PCL-CaSO<sub>4</sub> at the same time point.

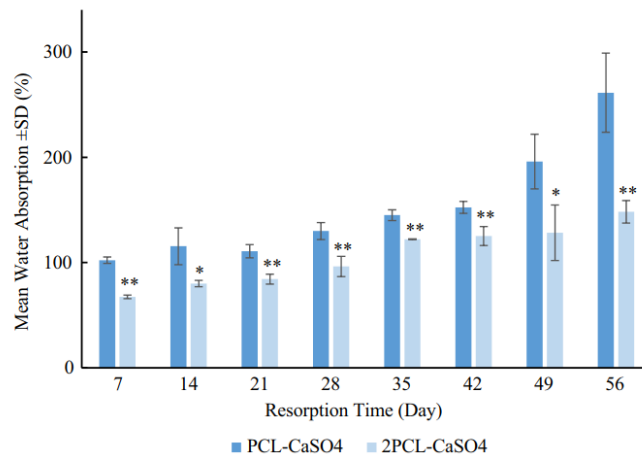


**Fig. 9** – Water absorption (Mean ± SD) for PCL-CaSO<sub>4</sub> and 2PCL-CaSO<sub>4</sub> scaffolds following resorption up to 56 days. \* P-value < 0.05 and \*\* P-value < 0.001, indicating a significant difference between PCL-CaSO<sub>4</sub> and 2PCL-CaSO<sub>4</sub> at the same time point.

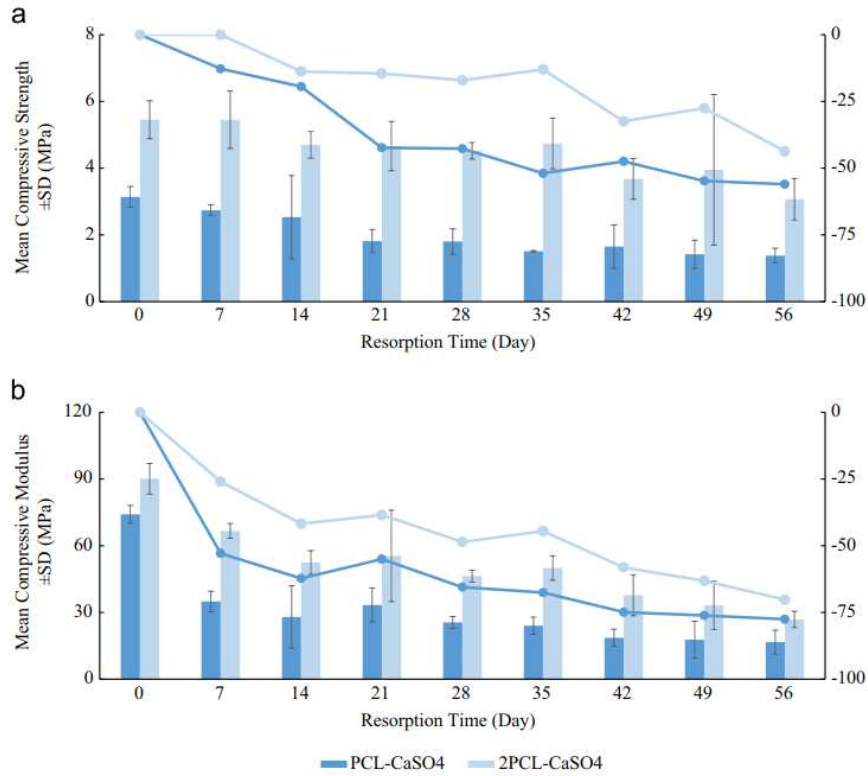


**Fig. 10 – (a) Compressive strength and (b) compressive modulus (Mean  $\pm$  SD) for PCL-CaSO<sub>4</sub> and 2PCL-CaSO<sub>4</sub> scaffolds following resorption up to 56 days. The average percentage change of the properties at each time point is also shown as line chart referring to the labelled secondary y-axis.**

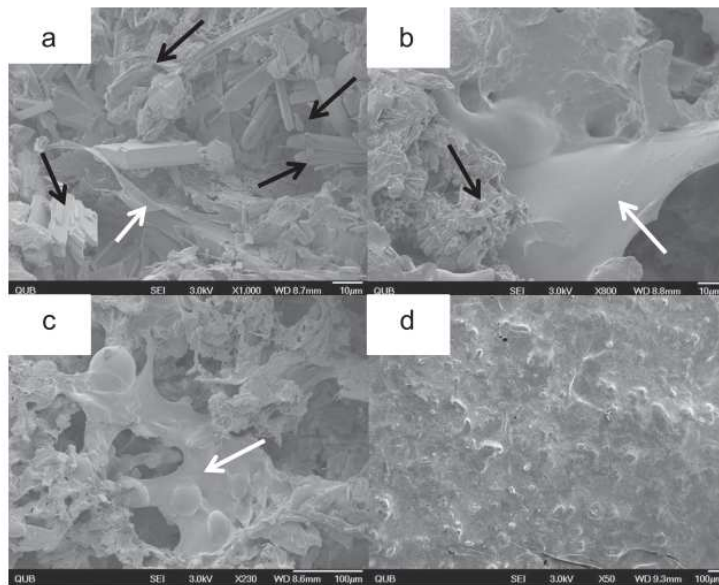


**Fig. 11 – SEM of the cross section of (a) PCL-CaSO<sub>4</sub> after 7 days resorption (1000  $\times$ ); (b) the cross section of 2PCL-CaSO<sub>4</sub> after 7 days resorption (800  $\times$ ); (c) the cross section of 2PCL-CaSO<sub>4</sub> after 56 days resorption (230  $\times$ ); and the surface of (d) PCL-CaSO<sub>4</sub> after 56 days resorption (500  $\times$ ). White arrows indicate PCL films and black arrows indicate CaSO<sub>4</sub> precipitates.**

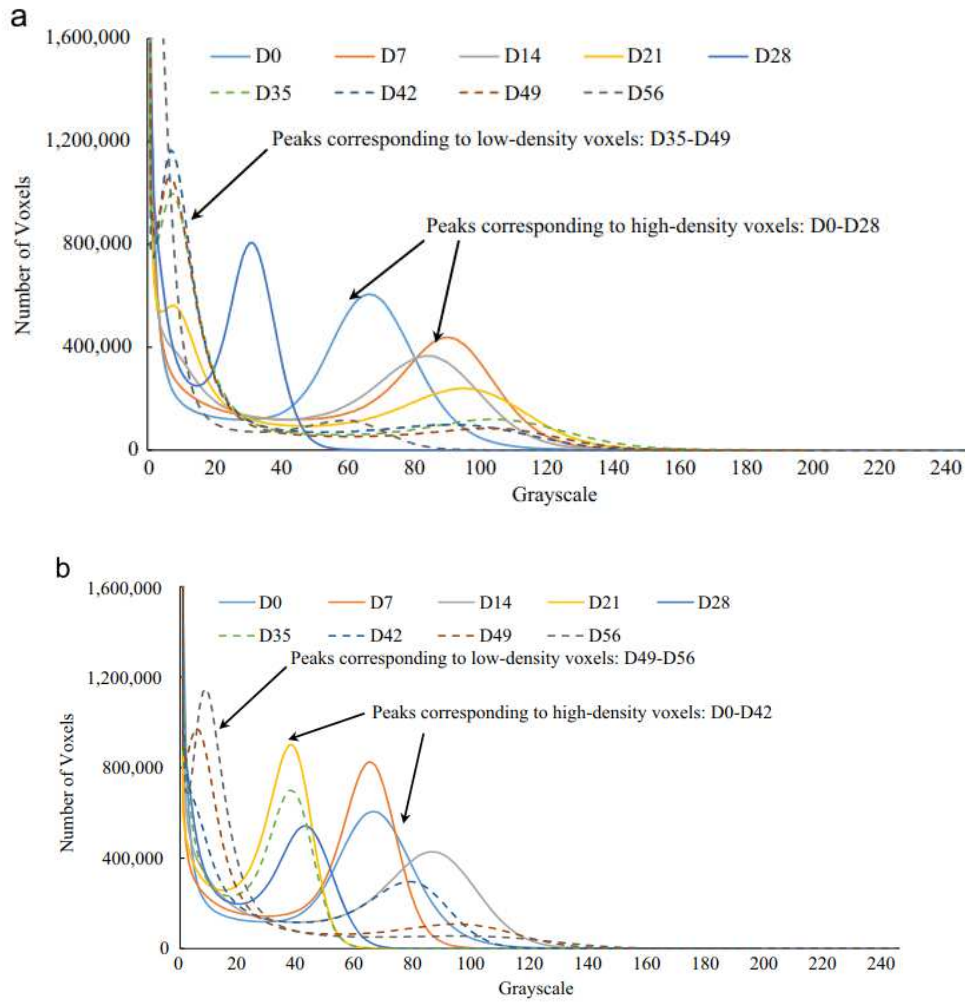


Fig. 12 – Grayscale histograms for  $\mu$ -CT results of (a) PCL-CaSO<sub>4</sub> and (b) 2PCL-CaSO<sub>4</sub> scaffolds following resorption up to 56 days.

**Table 1 – Three grayscale ranges for the  $\mu$ -CT results of resorption and the corresponding phase for each grayscale range.**

| Grayscale range | Corresponding phase    |
|-----------------|------------------------|
| 0–5             | Empty spaces           |
| 5–25            | Low-density materials  |
| 25–255          | High-density materials |

**Table 2 – Binary images of the cross sections of PCL-CaSO<sub>4</sub> and 2PCL-CaSO<sub>4</sub> at four time points of resorption (Day 0, 7, 28 and 56). The binary images were obtained from the reconstruction image using thresholding at two levels: 25–255 and 5–25. Pixels having grayscale in the range are in black. Scale bar=2 mm.**

| Resorption Time (Day) | PCL-CaSO <sub>4</sub>   |                       | 2PCL-CaSO <sub>4</sub>  |                       |
|-----------------------|-------------------------|-----------------------|-------------------------|-----------------------|
|                       | Grayscale Range: 25-255 | Grayscale Range: 5-25 | Grayscale Range: 25-255 | Grayscale Range: 5-25 |
| 0                     |                         |                       |                         |                       |
| 7                     |                         |                       |                         |                       |
| 28                    |                         |                       |                         |                       |
| 56                    |                         |                       |                         |                       |

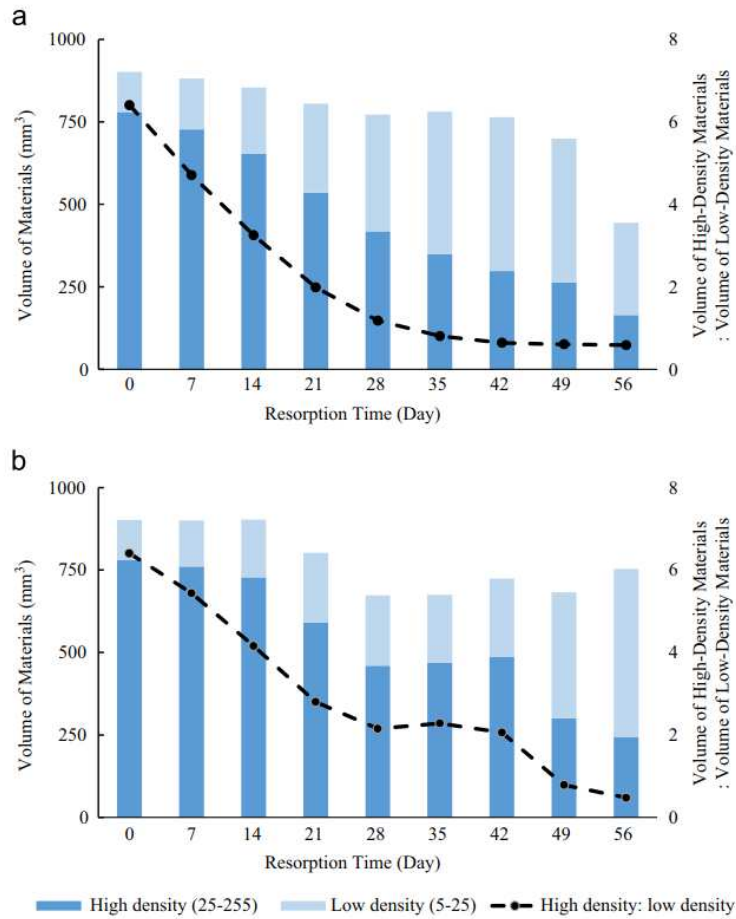


**Fig. 13 – Volume of materials for (a) PCL-CaSO<sub>4</sub> and (b) 2PCL-CaSO<sub>4</sub> scaffolds following resorption up to 56 days, determined via  $\mu$ -CT analysis. Volume of high-density materials, volume of low-density materials, and volume ratio of high-density materials to low-density materials were shown.**

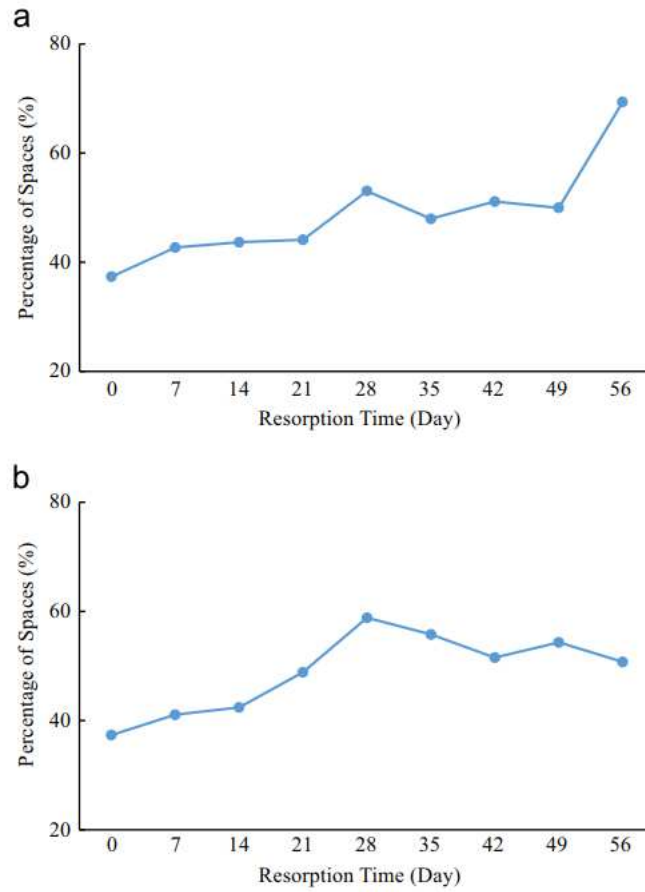


**Fig. 14 – Percentage of spaces for (a) PCL-CaSO<sub>4</sub> and (b) 2PCL-CaSO<sub>4</sub> scaffolds following resorption up to 56 days, determined via  $\mu$ -CT analysis.**

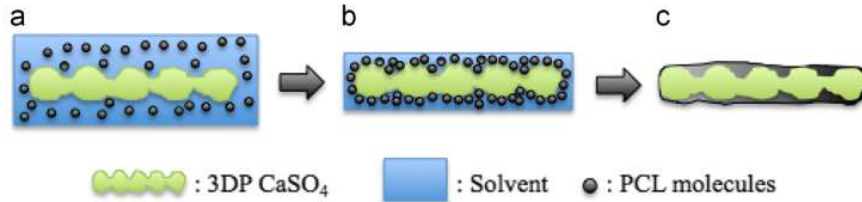


**Fig. 15 – Schematic of PCL coating on a 3DP ceramic surface. (a) CaSO<sub>4</sub> is immersed in the PCL coating solution. (b) During solvent evaporation, PCL molecules gradually adhere to the surface. (c) After solvent evaporation, a PCL layer was formed on the CaSO<sub>4</sub> surface, filling the gap in the regions of weak bonding.**